Published for SISSA by Springer

Received: *September 9, 2016*
Accepted: *February 19, 2017*
Published: *February 28, 2017*

Transverse-momentum resummation for Higgs boson pair production at the LHC with top-quark mass effects

Giancarlo Ferrera[a] **and João Pires**[b]

[a] *Dipartimento di Fisica, Università di Milano and INFN, Sezione di Milano, I-20133 Milan, Italy*
[b] *Max-Planck-Institute for Physics, Föhringer Ring 6, 80805 München, Germany*

E-mail: giancarlo.ferrera@mi.infn.it, pires@mpp.mpg.de

Abstract: We consider Higgs boson pair production via gluon fusion in hadronic collisions. We report the calculation of the transverse-momentum (q_T) distribution of the Higgs boson pair with top-quark mass (M_t) effects fully taken into account. At small values of q_T we resum the logarithmically-enhanced perturbative QCD contributions up to next-to-leading logarithmic (NLL) accuracy. At intermediate and large values of q_T we consistently combine resummation with the $\mathcal{O}(\alpha_S^3)$ fixed-order results. After integration over q_T, we recover the next-to-leading order (NLO) result for the inclusive cross section with full dependence on M_t. We present illustrative numerical results at LHC energies, together with an estimate of the corresponding perturbative uncertainties, and we study the impact of the top-quark mass effects.

Keywords: NLO Computations, QCD Phenomenology

ArXiv ePrint: 1609.01691

doi:10.1007/JHEP02(2017)139

JHEP02(2017)139

Contents

JHEP02(2017)139

1 Introduction

Since the discovery of the Higgs boson (H) [1, 2] during Run I of the Large Hadron Collider (LHC), it became a physics goal for Run II and future high-energy collider facilities to complete our understanding of the electroweak symmetry breaking mechanism of the Standard Model (SM). The study with increased precision of the couplings between the Higgs boson and the SM particles shows a determination of the couplings to vector bosons and heavy fermions compatible with the SM values with an overall 15% to 20% uncertainty [3–5]. The results obtained in refs. [3–5] concern single Higgs boson production.

In order to probe the Higgs boson self couplings one can consider the process of double Higgs boson (HH) production [6–11]. In this case, similarly to single Higgs boson production, the main production mechanism is driven by gluon fusion. At the leading order (LO), the two Higgs bosons can couple to a heavy-quark loop via a box diagram or, via the trilinear Higgs self-coupling, to an off-shell Higgs boson produced by a triangular heavy-quark loop. For this reason, the observation of Higgs boson pair production gives access to a direct extraction of the Higgs trilinear self-coupling and to the reconstruction of the Higgs boson potential [12–17].

Predictions for double Higgs boson production in gluon fusion at LO were obtained in refs. [18–20] including full top-quark mass (M_t) effects. However, since the gluon fusion mechanism for HH production is a loop induced process, the next-to-leading order (NLO) QCD corrections were first obtained in the heavy top quark limit $M_t \to \infty$ [21] using the Higgs effective field theory (HEFT). In this approximation the top-quark mass is regarded much larger than any other scale in the process and the top quark is integrated out at the Lagrangian level. This significantly simplifies the calculation of the NLO corrections since the top-quark loops shrink to a point-like interaction of the Higgs bosons with gluons. More recently, next-to-next-to-leading order (NNLO) predictions for HH production in the HEFT have been completed in refs. [22–25]. Threshold resummation up to next-to-next-to-leading logarithmic (NNLL) accuracy in the HEFT has been performed in refs. [26] and [27] matching the resummed results respectively with NLO and NNLO fixed-order calculations.

However, Higgs boson pairs are produced with an invariant mass (M_{HH}) which is above the top-quark mass threshold where the validity of the HEFT description breaks down. Therefore, various approximations to include finite M_t effects beyond LO have been performed in the literature. In the so-called "Born-improved HEFT" approximation a reweighting of the NLO HEFT result is performed using a factor B_{FT}/B_{HEFT}, where B_{FT} and B_{HEFT} denote the LO matrix element squared in the full theory and in the HEFT respectively [21]. In the NLO calculation in refs. [28, 29] the top-quark mass dependence is fully taken into account in the real emission correction, while the virtual amplitude is computed in the heavy top quark limit and reweighted by the Born-improved factor. HEFT results at NLO and NNLO improved by an expansion in $1/M_t^2$ have been obtained in refs. [24, 30–32].

The NLO calculation including the full top-quark mass effects in both the real and virtual corrections has been performed only recently in refs. [33, 34]. It shows that the total cross section is about 14% smaller than the one obtained within the Born-improved HEFT approximation and that for values of the Higgs boson pair invariant mass beyond $M_{HH} \sim 500\,\text{GeV}$, the top-quark mass effects lead to a reduction of the differential cross section by about 20-30% with respect to the same approximation. Therefore, in order to get reliable predictions for the Higgs boson pair production cross section and corresponding distributions, it is important to include the full top-quark mass dependence.

Among the various kinematical distributions, a particularly significant role is played by the transverse-momentum (q_T) spectrum of the Higgs boson pair. A precise description of this observable is important to improve the statistical significance in the experimental searches and therefore, it is essential to carefully investigate the theoretical uncertainties dominated by the higher-order QCD corrections. In the large q_T region ($q_T \sim M_{HH}$) fixed-order calculations are theoretically justified. However, in the small q_T region ($q_T \ll M_{HH}$) the reliability of the fixed-order perturbative expansion is spoiled by the presence of large logarithmic terms of the type $\alpha_S^n \log^m(M_{HH}^2/q_T^2)$ which make the fixed-order results divergent in the limit $q_T \to 0$. In order to obtain reliable predictions at small q_T, such large logarithmic contributions have to be systematically resummed to all orders [35–37]–[48]. At intermediate values of q_T the resummed and fixed order results can be consistently matched in order to get a uniform theoretical accuracy for the entire range of transverse momenta.

We have used the formalism introduced in refs. [44, 45] to perform the transverse momentum resummation for Higgs boson pair production up to next-to-leading logarithmic (NLL) accuracy, combining it with the NLO (i.e. $\mathcal{O}(\alpha_S^3)$) result with full top-quark mass dependence. The implementation of our calculation for the q_T spectrum was performed starting from the numerical code `HqT` [45, 49].

The paper is organised as follows. In section 2 we briefly review the resummation formalism of refs. [44, 45, 48]. In section 3 we present numerical fixed-order and resummed results for the transverse-momentum distribution of Higgs boson pairs and we study the scale dependence of our results in order to estimate the perturbative uncertainty of our predictions. We also comment on the size of the finite top-quark mass effects. In section 4 we present our conclusions.

JHEP02(2017)139

2 Transverse-momentum resummation

The resummation formalism used in this paper has been introduced in refs. [44, 45] and can be applied to a generic process where a high-mass system of non strongly-interacting particles is produced in hadronic collisions. In this section we briefly recall the main points of the formalism, by considering the specific case of the hadroproduction of Higgs boson pairs in gluon fusion. For a detailed discussion we refer to refs. [44–48].

The transverse-momentum differential cross section for this process can be written as:[1]

$$\frac{d\sigma_{HH}}{dq_T^2}(q_T, M, s) = \sum_{a_1,a_2} \int_0^1 dx_1 \int_0^1 dx_2 f_{a_1/h_1}(x_1, \mu_F^2) f_{a_2/h_2}(x_2, \mu_F^2) \times \frac{d\hat{\sigma}_{HH\,a_1a_2}}{dq_T^2}(q_T, M, \hat{s}; \alpha_S(\mu_R^2), \mu_R^2, \mu_F^2)\,, \tag{2.1}$$

where $f_{a/h}(x, \mu_F^2)$ ($a = g, q, \bar{q}$) are the parton densities of the colliding hadrons (h_1 and h_2), $d\hat{\sigma}_{HH\,a_1a_2}/dq_T^2$ are the partonic cross sections, $M = M_{HH}$ is the invariant mass of the Higgs boson pair, s ($\hat{s} = x_1x_2s$) is the hadronic (partonic) centre-of-mass energy, μ_R and μ_F are respectively the renormalisation and factorisation scale.

The partonic cross section is decomposed as follows: $d\hat{\sigma}_{HH\,a_1a_2} = d\hat{\sigma}^{(\mathrm{res.})}_{HH\,a_1a_2} + d\hat{\sigma}^{(\mathrm{fin.})}_{HH\,a_1a_2}$. The 'resummed' component, $d\hat{\sigma}^{(\mathrm{res.})}_{HH\,a_1a_2}$, contains all the logarithmically-enhanced contributions at small q_T which have to be evaluated to all orders in α_S and the 'finite' component, $d\hat{\sigma}^{(\mathrm{fin.})}_{HH\,a_1a_2}$, is free of such contributions.

The resummation procedure is carried out in the impact-parameter (b) space. The resummed component is obtained by performing the inverse Bessel transformation with respect to the impact parameter:

$$\frac{d\hat{\sigma}^{(\mathrm{res.})}_{HH\,a_1a_2}}{dq_T^2}(q_T, M, \hat{s}; \alpha_S(\mu_R^2), \mu_R^2, \mu_F^2) = \frac{M^2}{\hat{s}} \int_0^\infty db\, \frac{b}{2} J_0(bq_T) \mathcal{W}^{HH}_{a_1a_2}(b, M, \hat{s}; \alpha_S(\mu_R^2), \mu_R^2, \mu_F^2)\,, \tag{2.2}$$

where $J_0(x)$ is the 0th-order Bessel function. The resummation structure of $\mathcal{W}^{HH}_{a_1a_2,\,N}$ can be factorised and organised in exponential form by considering the Mellin N-moments $\mathcal{W}_N$ of $\mathcal{W}$ with respect to $z = M^2/\hat{s}$ at fixed M:[2]

$$\mathcal{W}^{HH}_N(b, M; \alpha_S(\mu_R^2), \mu_R^2, \mu_F^2) = \mathcal{H}^{HH}_N\left(M, \alpha_S(\mu_R^2); M^2/\mu_R^2, M^2/\mu_F^2, M^2/Q^2\right) \times \exp\{\mathcal{G}_N(\alpha_S(\mu_R^2), \tilde{L}; M^2/\mu_R^2, M^2/Q^2)\}\,, \tag{2.3}$$

where we have defined the logarithmic expansion parameter $\tilde{L} = \ln\left(Q^2b^2/b_0^2 + 1\right)$, and $b_0 = 2e^{-\gamma_E}$ ($\gamma_E = 0.5772\ldots$ is the Euler number). The resummation scale Q [45] parameterises the arbitrariness in the separation (factorisation) between finite and logarithmically-enhanced terms. Variations of Q around the hard scale M can be used to estimate the effect of uncalculated higher-order logarithmic contributions.

The *universal* (process independent) form factor $\exp\{\mathcal{G}_N\}$ includes all the large logarithmic terms $\alpha_S^n \tilde{L}^m$, with $1 \le m \le 2n$ that order-by-order in α_S are logarithmically

[1] In this section we denote with $d\hat{\sigma}_{HH}/dq_T^2$ the double differential cross section $M^2 d\hat{\sigma}_{HH}/dM^2 dq_T^2$.

[2] Here, to simplify the notation, flavour indices are understood.

JHEP02(2017)139

divergent as $b \to \infty$. The exponent $\mathcal{G}_N$ can systematically be expanded in powers of $\alpha_S \equiv \alpha_S(\mu_R^2)$ as follows:

$$\mathcal{G}_N(\alpha_S, \tilde{L}; M^2/\mu_R^2, M^2/Q^2) = \tilde{L}\, g^{(1)}(\alpha_S \tilde{L}) + g_N^{(2)}(\alpha_S \tilde{L}; M^2/\mu_R^2, M^2/Q^2) + \frac{\alpha_S}{\pi} g_N^{(3)}(\alpha_S \tilde{L}; M^2/\mu_R^2, M^2/Q^2) + \dots , \tag{2.4}$$

where the term $\tilde{L}\, g^{(1)}$ collects the leading logarithmic (LL) contributions, the function $g_N^{(2)}$ includes the NLL contributions, $g_N^{(3)}$ controls the NNLL terms and so forth. The logarithmic variable $\tilde{L}$ is equivalent to $L = \ln\left(Q^2 b^2/b_0^2\right)$ when $Qb \gg 1$ (i.e. small values of q_T), but it leads to a behaviour of the form factor at small values of b such that $\tilde{L} \to 0$ and $\exp\{\mathcal{G}_N\} \to 1$ when $Qb \ll 1$. The logarithmic expansion with respect to $\tilde{L}$ thus reduces the impact of large and unjustified resummed contributions in the small-b region (i.e. at large values of q_T), and it acts as a perturbative unitarity constraint since it allows us to exactly recover the fixed-order value of the total cross section upon integration over q_T.

The hard-collinear function $\mathcal{H}_N^{HH}$ fully encodes the process dependence of the resummation factor $\mathcal{W}_N^{HH}$ and it includes all the perturbative terms that behave as constants in the limit $b \to \infty$. It has a customary perturbative expansion:

$$\mathcal{H}_N^{HH}(M, \alpha_S; M^2/\mu_R^2, M^2/\mu_F^2, M^2/Q^2) = \sigma_{HH}^{(0)}(M) \left[1 + \frac{\alpha_S}{\pi}\, \mathcal{H}_N^{HH\,(1)}(M^2/\mu_F^2, M^2/Q^2) + \left(\frac{\alpha_S}{\pi}\right)^2 \mathcal{H}_N^{HH\,(2)}(M^2/\mu_R^2, M^2/\mu_F^2, M^2/Q^2) + \dots\right], \tag{2.5}$$

where $\sigma_{HH}^{(0)}$ is the Born-level partonic cross section for the process $gg \to HH$.

The general structure of the hard-collinear function $\mathcal{H}_N^F$ has been obtained in ref. [48], where it is shown that the process dependent contribution to $\mathcal{H}_N^F$ can be embodied in a single perturbative hard factor which is directly related to the finite part of the virtual amplitude of the corresponding process. The process independent part of the hard-collinear function $\mathcal{H}_N^F$ has been explicitly computed up to NNLO in refs. [50, 51]. For HH production the NLO corrections in the full theory were recently calculated [33, 34]. From the values of the virtual amplitude with full top-quark mass dependence computed in refs. [33, 34] we extracted numerically the process dependent contribution to the NLO coefficient $\mathcal{H}_N^{HH\,(1)}$.

We now consider the finite component of the cross section. Since it does not contain large logarithmic terms, it can be computed at fixed order in perturbation theory starting from the standard fixed-order results and subtracting the expansion of the resummed component at the same perturbative order [45].

In summary, the resummation at NLL+NLO accuracy is obtained by including the functions $g^{(1)}$, $g_N^{(2)}$ and the coefficient $\mathcal{H}_N^{HH(1)}$ in the resummed component, and by computing the finite component at first order (i.e. at $\mathcal{O}(\alpha_S^3)$).[3] We note that the NLL+NLO result includes the *full* NLO perturbative contribution in the small-q_T region and that the NLO result for the total cross section is exactly recovered upon integration over q_T of the differential cross section $d\sigma/dq_T$ at NLL+NLO accuracy.

[3] This matching procedure coincides with that of refs. [45, 52]. We note however that here we are using different labels. The fixed-order label NLO used here directly refers to the perturbative accuracy in the small-q_T region and of the total cross section, while the labels LO and NLO used in refs. [45, 52] refer to the perturbative accuracy in the large-q_T region.

JHEP02(2017)139

3 Numerical results for *HH* production at the LHC

In this section we consider Higgs pair production via gluon fusion in pp collisions at the centre-of-mass energy of $\sqrt{s} = 14\,\text{TeV}$. We first show the fixed-order results which are valid in the large q_T region and then we present our resummed prediction at NLL+NLO focusing on the small q_T region. We include the full dependence on the top-quark mass and we comment on the size of the M_t effects.

The hadronic cross section is computed using the PDF4LHC15 NLO parton densities [53–58] with α_S evaluated at 2-loop order and $\alpha_S(m_Z^2) = 0.118$ and we consider $N_f = 5$ flavours of light quarks in the massless approximation. We set the central value of the renormalisation, factorisation and resummation scales at $\mu_R = \mu_F = Q = M_{HH}/2$. The Higgs boson and top-quark masses have been set to $M_H = 125\,\text{GeV}$ and $M_t = 173\,\text{GeV}$ respectively, and the top quark and Higgs boson widths have been set to zero.

Bottom-quark mass effects in the double Higgs boson total cross section contribute well below 1% level and have been neglected in the present study. We thus have a two-scale problem with $q_T \ll M$, where M is the *hard* scale of the process $M \sim M_{HH}$ and the top-quark mass is of the same order of the hard scale. This fact justifies the application of the standard q_T resummation formalism to compute the HH q_T spectrum with finite top-quark mass effects.[4]

We start the presentation of our numerical results by considering the calculation at fixed order. As explained in the previous section we performed the calculation of the double Higgs boson q_T spectrum at first order in QCD (i.e. $\mathcal{O}(\alpha_S^3)$). The relevant partonic subprocesses are $gg \to HHg$, $qg \to HHq$, $\bar{q}g \to HH\bar{q}$ and $q\bar{q} \to HHg$ and we have generated all the relevant one-loop amplitudes using `GoSam` [60, 61] retaining the full top-quark mass dependence. The corresponding matrix elements in the HEFT have been computed analytically. The phase space integration was performed using the `CUBA` library [62].

In figure 1 (left panel) we present the double Higgs boson q_T spectrum for an invariant mass in the range $300 < M_{HH} < 500\,\text{GeV}$ at the LHC ($\sqrt{s} = 14\,\text{TeV}$). We show the first order prediction in the full theory which includes the exact top-quark mass dependence (blue solid line) and in the HEFT (black dotted). In addition, we present also the approximation obtained by reweighting the HEFT result by the Born-level matrix elements for HH production with the full top-quark mass dependence (red dashed). The reweighting is performed at the matrix element level using the initial-initial antenna phase space mapping [63] to generate a Higgs boson pair Born-like configuration from the real-emission kinematics.

We show the scale dependence band (blue solid) of the full theory result which is obtained by varying independently the renormalisation and factorisation scales by a factor 2 around their central value, with the constraint $1/2 \leq \mu_R/\mu_F \leq 2$. The scale dependence band is about $\pm 35\%$ at small q_T, and it slightly increases up to $\pm 40\%$ at $q_T \sim 400 - 500\,\text{GeV}$. We observe that the band is rather large and flat. This is not unexpected since the bulk of the scale dependence is due to the μ_R dependence which is driven by the overall factor $\alpha_S(\mu_R)^3$.

[4] We note that the case of single Higgs boson production is different, since bottom-quark mass effects are sizeable and their inclusion leads to a three-scale problem [59].

JHEP02(2017)139

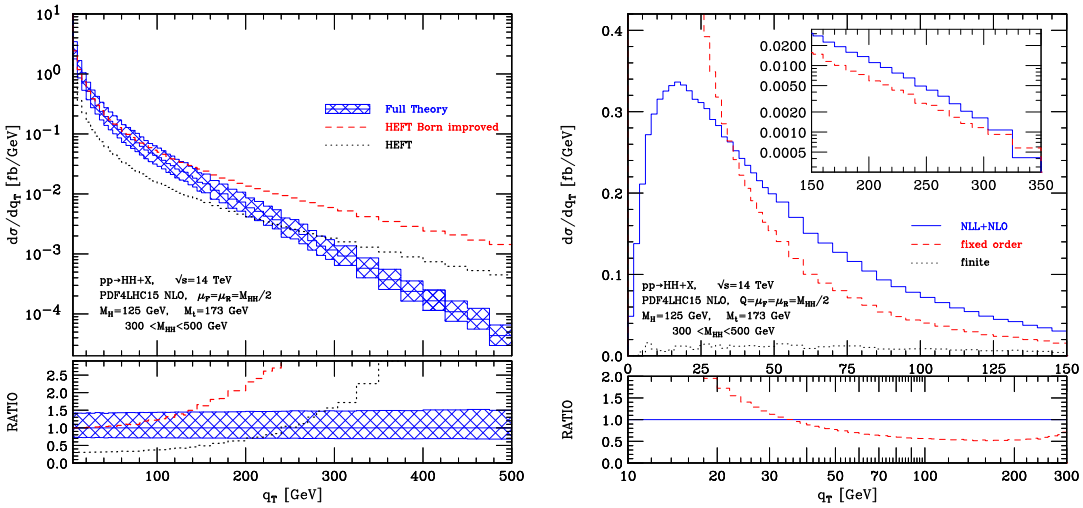

Figure 1. The q_T spectrum of Higgs boson pairs at the LHC ($\sqrt{s} = 14\,\text{TeV}$). Left panel: fixed-order prediction at $\mathcal{O}(\alpha_S^3)$ accuracy in the full theory (blue solid), HEFT (black dotted) and Born-improved reweighted HEFT (red dashed). The band is obtained by varying μ_R and μ_F as described in the text. Right panel: resummed prediction at NLL+NLO accuracy in the full theory. The resummed result (blue solid) is compared to the corresponding fixed-order result (red dashed) and to the finite component (black dotted). The lower panels show the ratios with respect to the central value of the full theory result.

By comparing the effective theory and the full theory results we observe that the pure HEFT calculation gives a poor approximation of the full theory spectrum for the entire range of q_T (the two predictions accidentally cross each other for $q_T \sim 250\,\text{GeV}$). The Born-improved reweighted HEFT result gives a good approximation of the exact calculation in the small q_T region ($q_T \lesssim 50\,\text{GeV}$) where however both results diverge logarithmically. This is expected since in the small q_T limit the phase space is restricted to soft and collinear emissions and in this limit the fixed-order cross section factorises into the Born contribution and process independent logarithmic terms. At larger q_T ($q_T \gtrsim 50\,\text{GeV}$), the agreement between the Born-improved HEFT and the full theory result rapidly deteriorates. The top-quark mass effects in the loop diagrams produce deviations in the fixed order q_T spectrum of about $20 - 25\%$ at $q_T \sim 100\,\text{GeV}$ and $80 - 100\%$ at $q_T \sim 175\,\text{GeV}$. The q_T spectrum in the Born-improved HEFT approximation is much harder than in the full theory and generates an unphysical tail at large q_T.

We now turn to present the resummed results. In figure 1 (right panel) we compare the NLL+NLO spectrum (blue solid line) at the default scales ($\mu_F = \mu_R = Q = M_{HH}/2$) with the fixed-order result (red dashed). The finite component is also shown for comparison (black dotted). In the inset plot of the figure it is shown the region from intermediate to large values of q_T. We observe that while the fixed-order calculation diverges at $q_T \to 0$, the resummation leads to a well-behaved distribution: it vanishes as $q_T \to 0$, has a kinematical peak at $q_T \sim 18\,\text{GeV}$ and tends to the corresponding fixed-order result for $q_T \sim M_{HH}$. The finite component vanishes as $q_T \to 0$ and gives a contribution to the NLL+NLO result

JHEP02(2017)139

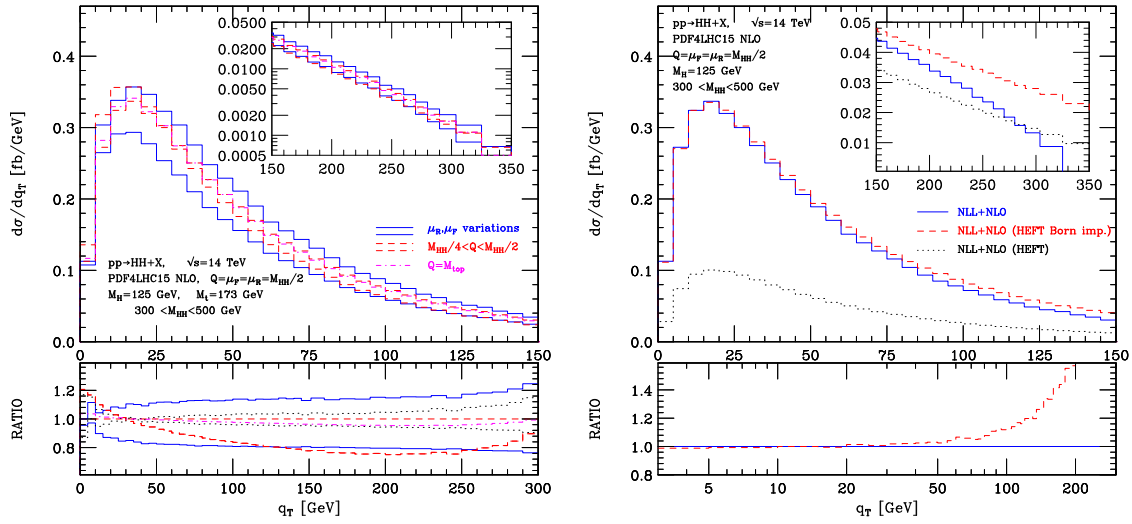

Figure 2. The q_T spectrum of Higgs boson pairs at the LHC ($\sqrt{s} = 14\,\text{TeV}$). Left panel: scale variation bands for the NLL+NLO result in the full theory. The bands are obtained by varying μ_R and μ_F and Q as described in the text. Right panel: resummed prediction at NLL+NLO accuracy in the full theory (blue solid), HEFT (black dotted) and Born-improved reweighted HEFT (red dashed). The lower panels show the ratios with respect to the central value of the full theory result.

that is around 4% in the peak region and it increases to about 15% at $q_T \sim 125\,\text{GeV}$ and 30% at $q_T \sim 200\,\text{GeV}$. We notice that in a wide region of intermediate values of q_T the difference between the NLL+NLO and the fixed-order result is quite large (around $40-50\%$ for $80 \lesssim q_T \lesssim 250\,\text{GeV}$), thus indicating that the effect of the logarithmic terms included in the resummation is important even outside the small-q_T region. The contribution of the finite component sizeably increases at large values of q_T ($q_T \sim M_{HH}$) and the resummed spectrum approaches the fixed order prediction. We have checked the numerical accuracy of our calculation by computing the integral over q_T of the NLL+NLO resummed spectrum. The result is in agreement with the value of the NLO total cross section calculated in refs. [33, 34] at the percent level, thus proving that the uncertainty associated to the numerical extraction of the $\mathcal{H}_N^{HH\,(1)}$ coefficient is completely under control.

We now discuss the scale dependence of the NLL+NLO result. As previously discussed the resummation formalism we are using is strictly valid for a two-scale problem with the resummation scale of the order of the top-quark mass. For this reason we explicitly avoided values of the resummation scale parametrically too large with respect to the top-quark mass M_t. In figure 2 (left panel) we show the resummation scale dependence band (red dashed lines) obtained by varying Q in the region $M_{HH}/4 \leq Q \leq M_{HH}/2$ at fixed values of μ_R and μ_F ($\mu_R = \mu_F = M_{HH}/2$). The resummation scale dependence is about $\pm 3\%$ at the peak, decreases to about $\pm 1.5\%$ at $q_T \sim 30\,\text{GeV}$ and increases again to about $\pm 12\%$ at $q_T \sim 200\,\text{GeV}$.

Additionally we show in figure 2 (left panel) the resummed prediction for the resummation scale choice $Q = M_{\text{top}}$ (magenta dot-dashed line) and we quantitatively estimated the effect of this choice. We observe no significant differences with respect to the choice

JHEP02(2017)139

$Q = M_{HH}/2$. The percentual difference with respect to our default value ($Q = M_{HH}/2$) is around 1% at the peak, it decreases to few permille at $q_T \sim 30\,\text{GeV}$, it increases to 2% at $q_T \sim 100\,\text{GeV}$ and it remains $\lesssim 4\%$ for $100 \lesssim q_T \lesssim 300\,\text{GeV}$. This quantitative effect is widely covered by the resummation scale uncertainty band and can be explained by the fact that the *HH* cross section is peaked at an invariant mass of the order of $M_{HH} \simeq 400\,\text{GeV}$ (for which $M_{HH}/2 \approx M_{\text{top}}$) [33, 34].

In figure 2 (left panel) we also considered the renormalisation and factorisation scale dependence band (blue solid) obtained by varying independently μ_R and μ_F by a factor 2 around their central value (with the constraint $1/2 \leq \mu_R/\mu_F \leq 2$) at fixed value of the resummation scale ($Q = M_{HH}/2$). The μ_R and μ_F scale dependence band is about $\pm 10\%$ at the peak and it increases to about $\pm 12\%$ at $q_T \sim 30\,\text{GeV}$, to about $\pm 17\%$ at $q_T \sim 100\,\text{GeV}$ and to about $\pm 20\%$ at $q_T \gtrsim 250\,\text{GeV}$. We observe that the size of the μ_R and μ_F band is larger than the Q band for a wide region of q_T ($q_T \lesssim 250\,\text{GeV}$). By comparing the μ_R and μ_F scale dependence bands of fixed order and resummed calculations, we observe that the resummed scale dependence band is not flat and its size is smaller than the fixed-order one at small and intermediate values of q_T ($q_T \lesssim 250\,\text{GeV}$). This behaviour is not unexpected since the NLL+NLO resummed result, contrary to the fixed-order case, includes the full NLO correction in the small-q_T region and satisfies the NLO unitarity constraint described at the end of section 2 (see the discussion after eq. (2.4)) and these NLO effects are spread on a region from small to intermediate values of q_T. Nevertheless we point out that the μ_R and μ_F scale dependence is only a part of the perturbative uncertainty of the resummed prediction which includes also the resummation scale dependence.

We add a comment on the relation between the scale variation bands and the normalisation of the resummed q_T spectra which is given by the corresponding NLO total cross section. On the one hand, the total cross section does not depend on the resummation scale. For this reason, the corresponding uncertainty band is independent on normalisation effects. On the other hand, the μ_R and μ_F scale variation band depends on normalisation effects and can be substantially reduced if we consider the *normalised* q_T spectrum, $1/\sigma \times d\sigma/dq_T$ (i.e. if we are interested only on the *shape* of the q_T distribution and not on its normalisation). The μ_R and μ_F scale dependence band for the normalised q_T spectrum is shown in the lower left panel in figure 2 (black dotted lines), and we observe that it becomes smaller than the resummation scale uncertainty band for the entire q_T range.

We conclude this section with an assessment of the size of the finite top-quark mass effects which are included in our calculation. In order to study the impact of the M_t effects we computed the resummed spectrum also in the HEFT approximation and in the Born-improved HEFT (the latter approximation was obtained by reweighting the HEFT result with the Born-improved factor at a differential level).[5] In figure 2 (right panel) we compare the NLL+NLO prediction in the full theory with exact M_t dependence (blue solid line), with the pure HEFT (black dotted) and with the Born-improved HEFT (red dashed) results. We observe, similarly to the fixed-order case, that the Born-improved HEFT gives

[5] We stress that the full theory result contains the complete finite M_t effects both in the resummed part, through the Born-level partonic cross section $\sigma^{(0)}_{HH}$ and the NLO coefficient $\mathcal{H}_N^{HH\,(1)}$ (see eq. (2.5)), and in the finite component.

JHEP02(2017)139

a good approximation (within 5% accuracy) of the full theory result for $q_T \lesssim 70\,\text{GeV}$.[6] At higher values of q_T we observe that the finite top mass effects are large and have a strong q_T dependence. The effect is about 12% at $q_T \sim 100\,\text{GeV}$, about 60% at $q_T \sim 200\,\text{GeV}$ and larger than 200% for $q_T \gtrsim 250\,\text{GeV}$, showing that the inclusion of the full top-quark mass dependence is essential to obtain a reliable description of the double Higgs boson q_T spectrum over a wide region of q_T.

4 Conclusions

We have considered Higgs boson pairs produced in gluon fusion in hadronic collisions and we performed the calculation of the transverse-momentum (q_T) distribution of the double Higgs boson system taking into account finite top-quark mass (M_t) effects.

At small values of q_T we have resummed the logarithmically-enhanced perturbative QCD contributions using the formalism introduced in refs. [44, 45]. We have presented the results of the resummed calculation at next-to-leading logarithmic accuracy (NLL), and we have combined them with the fixed-order computation at $\mathcal{O}(\alpha_S^3)$. Our calculation includes the complete next-to-leading order (NLO) contributions at small q_T and exactly reproduces the NLO total cross section with the full top-quark mass dependence upon integration over q_T.

We have presented illustrative numerical results in pp collisions at $\sqrt{s} = 14\,\text{TeV}$, performing a study of the scale dependence of our predictions to estimate the corresponding perturbative uncertainty. Comparing the NLL+NLO and fixed-order results, we have shown that the higher-order terms contained in the resummed calculation are essential to obtain reliable predictions at small q_T and give an important contribution ($\gtrsim 40-50\%$) to the fixed-order result, in a wide region of intermediate values of q_T ($q_T \lesssim 250\,\text{GeV}$). Finally, by comparing our results with the Born-improved Higgs effective field theory (HEFT) approximation in the $M_t \to \infty$ limit, we have quantified the size of the finite M_t effects which turn out to be large ($\gtrsim 60\%$) for $q_T \gtrsim 200\,\text{GeV}$ and very large ($\gtrsim 200\%$) for $q_T \gtrsim 250\,\text{GeV}$.

Our results show that both q_T resummation and finite top-quark mass effects are necessary to obtain reliable predictions for the double Higgs boson q_T spectrum over the full transverse momentum range.

Acknowledgments

We would like to thank Stefano Catani, Daniel de Florian, Massimiliano Grazzini, Gudrun Heinrich and Matthias Kerner for helpful discussions and comments on the manuscript. We also thank the authors of refs. [33, 34] for providing us the numerical values of the finite part of the two-loop virtual amplitude with full top-quark mass dependence. JP would like to thank also Tom Zirke for helpful discussions and Stephan Jahn and Johann Felix von Soden-Fraunhofen for their help with `GoSam`.

[6] We note that the Born-improved HEFT approximation works particularly well (within 1% accuracy) for q_T values around the peak. This agreement is not general and it depends on the particular Higgs boson pair invariant mass window. Considering Higgs boson pairs with an invariant mass in the range $350 < M_{HH} < 400\,\text{GeV}$ the agreement in the peak region is about 7%.

JHEP02(2017)139

References

[1] ATLAS collaboration, *Observation of a new particle in the search for the Standard Model Higgs boson with the ATLAS detector at the LHC*, *Phys. Lett.* **B 716** (2012) 1 [arXiv:1207.7214] [INSPIRE].

[2] CMS collaboration, *Observation of a new boson at a mass of 125 GeV with the CMS experiment at the LHC*, *Phys. Lett.* **B 716** (2012) 30 [arXiv:1207.7235] [INSPIRE].

[3] CMS collaboration, *Precise determination of the mass of the Higgs boson and tests of compatibility of its couplings with the standard model predictions using proton collisions at 7 and 8 TeV*, *Eur. Phys. J.* **C 75** (2015) 212 [arXiv:1412.8662] [INSPIRE].

[4] ATLAS collaboration, *Measurements of the Higgs boson production and decay rates and coupling strengths using pp collision data at $\sqrt{s} = 7$ and 8 TeV in the ATLAS experiment*, *Eur. Phys. J.* **C 76** (2016) 6 [arXiv:1507.04548] [INSPIRE].

[5] ATLAS and CMS collaborations, *Measurements of the Higgs boson production and decay rates and constraints on its couplings from a combined ATLAS and CMS analysis of the LHC pp collision data at $\sqrt{s} = 7$ and 8 TeV*, *JHEP* **08** (2016) 045 [arXiv:1606.02266] [INSPIRE].

[6] ATLAS collaboration, *Search For Higgs Boson Pair Production in the $\gamma\gamma b\bar{b}$ Final State using pp Collision Data at $\sqrt{s} = 8$ TeV from the ATLAS Detector*, *Phys. Rev. Lett.* **114** (2015) 081802 [arXiv:1406.5053] [INSPIRE].

[7] CMS collaboration, *Search for resonant pair production of Higgs bosons decaying to two bottom quark-antiquark pairs in proton-proton collisions at 8 TeV*, *Phys. Lett.* **B 749** (2015) 560 [arXiv:1503.04114] [INSPIRE].

[8] ATLAS collaboration, *Search for Higgs boson pair production in the $b\bar{b}b\bar{b}$ final state from pp collisions at $\sqrt{s} = 8$ TeV with the ATLAS detector*, *Eur. Phys. J.* **C 75** (2015) 412 [arXiv:1506.00285] [INSPIRE].

[9] ATLAS collaboration, *Searches for Higgs boson pair production in the $hh \to bb\tau\tau, \gamma\gamma WW^*, \gamma\gamma bb, bbbb$ channels with the ATLAS detector*, *Phys. Rev.* **D 92** (2015) 092004 [arXiv:1509.04670] [INSPIRE].

[10] CMS collaboration, *Search for two Higgs bosons in final states containing two photons and two bottom quarks in proton-proton collisions at 8 TeV*, *Phys. Rev.* **D 94** (2016) 052012 [arXiv:1603.06896] [INSPIRE].

[11] ATLAS collaboration, *Search for pair production of Higgs bosons in the $b\bar{b}b\bar{b}$ final state using proton–proton collisions at $\sqrt{s} = 13$ TeV with the ATLAS detector*, *Phys. Rev.* **D 94** (2016) 052002 [arXiv:1606.04782] [INSPIRE].

[12] M.J. Dolan, C. Englert and M. Spannowsky, *Higgs self-coupling measurements at the LHC*, *JHEP* **10** (2012) 112 [arXiv:1206.5001] [INSPIRE].

[13] J. Baglio, A. Djouadi, R. Gröber, M.M. Mühlleitner, J. Quevillon and M. Spira, *The measurement of the Higgs self-coupling at the LHC: theoretical status*, *JHEP* **04** (2013) 151 [arXiv:1212.5581] [INSPIRE].

JHEP02(2017)139

[14] F. Goertz, A. Papaefstathiou, L.L. Yang and J. Zurita, *Higgs Boson self-coupling measurements using ratios of cross sections*, *JHEP* **06** (2013) 016 [arXiv:1301.3492] [INSPIRE].

[15] V. Barger, L.L. Everett, C.B. Jackson and G. Shaughnessy, *Higgs-Pair Production and Measurement of the Triscalar Coupling at LHC(8,14)*, *Phys. Lett.* **B 728** (2014) 433 [arXiv:1311.2931] [INSPIRE].

[16] D.E. Ferreira de Lima, A. Papaefstathiou and M. Spannowsky, *Standard model Higgs boson pair production in the $(b\bar{b})$ $(b\bar{b})$ final state*, *JHEP* **08** (2014) 030 [arXiv:1404.7139] [INSPIRE].

[17] S. Dawson, A. Ismail and I. Low, *What's in the loop? The anatomy of double Higgs production*, *Phys. Rev.* **D 91** (2015) 115008 [arXiv:1504.05596] [INSPIRE].

[18] O.J.P. Eboli, G.C. Marques, S.F. Novaes and A.A. Natale, *Twin Higgs boson production*, *Phys. Lett.* **B 197** (1987) 269 [INSPIRE].

[19] E.W.N. Glover and J.J. van der Bij, *Higgs boson pair production via gluon fusion*, *Nucl. Phys.* **B 309** (1988) 282 [INSPIRE].

[20] T. Plehn, M. Spira and P.M. Zerwas, *Pair production of neutral Higgs particles in gluon-gluon collisions*, *Nucl. Phys.* **B 479** (1996) 46 [*Erratum ibid.* **B 531** (1998) 655] [hep-ph/9603205] [INSPIRE].

[21] S. Dawson, S. Dittmaier and M. Spira, *Neutral Higgs boson pair production at hadron colliders: QCD corrections*, *Phys. Rev.* **D 58** (1998) 115012 [hep-ph/9805244] [INSPIRE].

[22] D. de Florian and J. Mazzitelli, *Two-loop virtual corrections to Higgs pair production*, *Phys. Lett.* **B 724** (2013) 306 [arXiv:1305.5206] [INSPIRE].

[23] D. de Florian and J. Mazzitelli, *Higgs Boson Pair Production at Next-to-Next-to-Leading Order in QCD*, *Phys. Rev. Lett.* **111** (2013) 201801 [arXiv:1309.6594] [INSPIRE].

[24] J. Grigo, K. Melnikov and M. Steinhauser, *Virtual corrections to Higgs boson pair production in the large top quark mass limit*, *Nucl. Phys.* **B 888** (2014) 17 [arXiv:1408.2422] [INSPIRE].

[25] D. de Florian et al., *Differential Higgs Boson Pair Production at Next-to-Next-to-Leading Order in QCD*, *JHEP* **09** (2016) 151 [arXiv:1606.09519] [INSPIRE].

[26] D.Y. Shao, C.S. Li, H.T. Li and J. Wang, *Threshold resummation effects in Higgs boson pair production at the LHC*, *JHEP* **07** (2013) 169 [arXiv:1301.1245] [INSPIRE].

[27] D. de Florian and J. Mazzitelli, *Higgs pair production at next-to-next-to-leading logarithmic accuracy at the LHC*, *JHEP* **09** (2015) 053 [arXiv:1505.07122] [INSPIRE].

[28] R. Frederix et al., *Higgs pair production at the LHC with NLO and parton-shower effects*, *Phys. Lett.* **B 732** (2014) 142 [arXiv:1401.7340] [INSPIRE].

[29] F. Maltoni, E. Vryonidou and M. Zaro, *Top-quark mass effects in double and triple Higgs production in gluon-gluon fusion at NLO*, *JHEP* **11** (2014) 079 [arXiv:1408.6542] [INSPIRE].

[30] J. Grigo, J. Hoff, K. Melnikov and M. Steinhauser, *On the Higgs boson pair production at the LHC*, *Nucl. Phys.* **B 875** (2013) 1 [arXiv:1305.7340] [INSPIRE].

[31] J. Grigo, J. Hoff and M. Steinhauser, *Higgs boson pair production: top quark mass effects at NLO and NNLO*, *Nucl. Phys.* **B 900** (2015) 412 [arXiv:1508.00909] [INSPIRE].

JHEP02(2017)139

[32] G. Degrassi, P.P. Giardino and R. Gröber, *On the two-loop virtual QCD corrections to Higgs boson pair production in the Standard Model*, *Eur. Phys. J.* **C 76** (2016) 411 [arXiv:1603.00385] [INSPIRE].

[33] S. Borowka et al., *Higgs Boson Pair Production in Gluon Fusion at Next-to-Leading Order with Full Top-Quark Mass Dependence*, *Phys. Rev. Lett.* **117** (2016) 012001 [*Erratum ibid.* **117** (2016) 079901] [arXiv:1604.06447] [INSPIRE].

[34] S. Borowka et al., *Full top quark mass dependence in Higgs boson pair production at NLO*, *JHEP* **10** (2016) 107 [arXiv:1608.04798] [INSPIRE].

[35] Y.L. Dokshitzer, D. Diakonov and S.I. Troian, *On the Transverse Momentum Distribution of Massive Lepton Pairs*, *Phys. Lett.* **B 79** (1978) 269 [INSPIRE].

[36] G. Parisi and R. Petronzio, *Small Transverse Momentum Distributions in Hard Processes*, *Nucl. Phys.* **B 154** (1979) 427 [INSPIRE].

[37] G. Curci, M. Greco and Y. Srivastava, *QCD Jets From Coherent States*, *Nucl. Phys.* **B 159** (1979) 451 [INSPIRE].

[38] J.C. Collins and D.E. Soper, *Back-To-Back Jets in QCD*, *Nucl. Phys.* **B 193** (1981) 381 [*Erratum ibid.* **B 213** (1983) 545] [INSPIRE].

[39] J.C. Collins and D.E. Soper, *Back-To-Back Jets: Fourier Transform from B to K-Transverse*, *Nucl. Phys.* **B 197** (1982) 446 [INSPIRE].

[40] J.C. Collins, D.E. Soper and G.F. Sterman, *Transverse Momentum Distribution in Drell-Yan Pair and W and Z Boson Production*, *Nucl. Phys.* **B 250** (1985) 199 [INSPIRE].

[41] J. Kodaira and L. Trentadue, *Summing Soft Emission in QCD*, *Phys. Lett.* **B 112** (1982) 66 [INSPIRE].

[42] J. Kodaira and L. Trentadue, *Soft Gluon Effects In Perturbative Quantum Chromodynamics*, Report SLAC-PUB-2934 (1982).

[43] J. Kodaira and L. Trentadue, *Single Logarithm Effects in electron-Positron Annihilation*, *Phys. Lett.* **B 123** (1983) 335 [INSPIRE].

[44] S. Catani, D. de Florian and M. Grazzini, *Universality of nonleading logarithmic contributions in transverse momentum distributions*, *Nucl. Phys.* **B 596** (2001) 299 [hep-ph/0008184] [INSPIRE].

[45] G. Bozzi, S. Catani, D. de Florian and M. Grazzini, *Transverse-momentum resummation and the spectrum of the Higgs boson at the LHC*, *Nucl. Phys.* **B 737** (2006) 73 [hep-ph/0508068] [INSPIRE].

[46] G. Bozzi, S. Catani, D. de Florian and M. Grazzini, *Higgs boson production at the LHC: Transverse-momentum resummation and rapidity dependence*, *Nucl. Phys.* **B 791** (2008) 1 [arXiv:0705.3887] [INSPIRE].

[47] S. Catani and M. Grazzini, *QCD transverse-momentum resummation in gluon fusion processes*, *Nucl. Phys.* **B 845** (2011) 297 [arXiv:1011.3918] [INSPIRE].

[48] S. Catani, L. Cieri, D. de Florian, G. Ferrera and M. Grazzini, *Universality of transverse-momentum resummation and hard factors at the NNLO*, *Nucl. Phys.* **B 881** (2014) 414 [arXiv:1311.1654] [INSPIRE].

JHEP02(2017)139

[49] D. de Florian, G. Ferrera, M. Grazzini and D. Tommasini, *Transverse-momentum resummation: Higgs boson production at the Tevatron and the LHC*, *JHEP* **11** (2011) 064 [arXiv:1109.2109] [INSPIRE].

[50] S. Catani and M. Grazzini, *Higgs Boson Production at Hadron Colliders: Hard-Collinear Coefficients at the NNLO*, *Eur. Phys. J.* **C 72** (2012) 2013 [*Erratum ibid.* **C 72** (2012) 2132] [arXiv:1106.4652] [INSPIRE].

[51] S. Catani, L. Cieri, D. de Florian, G. Ferrera and M. Grazzini, *Vector boson production at hadron colliders: hard-collinear coefficients at the NNLO*, *Eur. Phys. J.* **C 72** (2012) 2195 [arXiv:1209.0158] [INSPIRE].

[52] G. Bozzi, S. Catani, G. Ferrera, D. de Florian and M. Grazzini, *Production of Drell-Yan lepton pairs in hadron collisions: Transverse-momentum resummation at next-to-next-to-leading logarithmic accuracy*, *Phys. Lett.* **B 696** (2011) 207 [arXiv:1007.2351] [INSPIRE].

[53] J. Butterworth et al., *PDF4LHC recommendations for LHC Run II*, *J. Phys.* **G 43** (2016) 023001 [arXiv:1510.03865] [INSPIRE].

[54] S. Dulat et al., *New parton distribution functions from a global analysis of quantum chromodynamics*, *Phys. Rev.* **D 93** (2016) 033006 [arXiv:1506.07443] [INSPIRE].

[55] L.A. Harland-Lang, A.D. Martin, P. Motylinski and R.S. Thorne, *Parton distributions in the LHC era: MMHT 2014 PDFs*, *Eur. Phys. J.* **C 75** (2015) 204 [arXiv:1412.3989] [INSPIRE].

[56] NNPDF collaboration, R.D. Ball et al., *Parton distributions for the LHC Run II*, *JHEP* **04** (2015) 040 [arXiv:1410.8849] [INSPIRE].

[57] S. Carrazza, S. Forte, Z. Kassabov, J.I. Latorre and J. Rojo, *An Unbiased Hessian Representation for Monte Carlo PDFs*, *Eur. Phys. J.* **C 75** (2015) 369 [arXiv:1505.06736] [INSPIRE].

[58] J. Gao and P. Nadolsky, *A meta-analysis of parton distribution functions*, *JHEP* **07** (2014) 035 [arXiv:1401.0013] [INSPIRE].

[59] M. Grazzini and H. Sargsyan, *Heavy-quark mass effects in Higgs boson production at the LHC*, *JHEP* **09** (2013) 129 [arXiv:1306.4581] [INSPIRE].

[60] G. Cullen et al., *Automated One-Loop Calculations with GoSam*, *Eur. Phys. J.* **C 72** (2012) 1889 [arXiv:1111.2034] [INSPIRE].

[61] G. Cullen et al., *GoSam-2.0: a tool for automated one-loop calculations within the Standard Model and beyond*, *Eur. Phys. J.* **C 74** (2014) 3001 [arXiv:1404.7096] [INSPIRE].

[62] T. Hahn, *CUBA: A Library for multidimensional numerical integration*, *Comput. Phys. Commun.* **168** (2005) 78 [hep-ph/0404043] [INSPIRE].

[63] A. Daleo, T. Gehrmann and D. Maître, *Antenna subtraction with hadronic initial states*, *JHEP* **04** (2007) 016 [hep-ph/0612257] [INSPIRE].

JHEP02(2017)139